THE JOURNAL OF BIOLOGICAL CHEMISTRY VOL. 284, NO. 25, pp. 16931–16938, June 19, 2009

Formation of Diapause Cyst Shell in Brine Shrimp, *Artemia parthenogenetica*, and Its Resistance Role in Environmental Stresses*[S]

Received for publication, March 25, 2009, and in revised form, April 4, 2009 Published, JBC Papers in Press, April 24, 2009, DOI 10.1074/jbc.M109.004051

Yu-Lei Liu[‡], Yang Zhao[‡], Zhong-Min Dai[‡], Han-Min Chen[§], and Wei-Jun Yang[‡¶1]

From the [‡]Institute of Cell Biology and Genetics and the [§]Equipment and Technology Service Platform, College of Life Sciences, Zhejiang University, and the [¶]State Conservation Center for Gene Resources of Wildlife and the Key Laboratory of Conservation Genetics and Reproductive Biology for Wild Animals of the Ministry of Education, Hangzhou, Zhejiang 310058, China

Artemia **has attracted much attention for its ability to produce encysted embryos wrapped in a protective shell when subject to extremely harsh environmental conditions. However, what the cyst shell is synthesized from and how the formative process is performed remains, as yet, largely unknown. Over 20 oviparous specifically expressed genes were identified through screening the subtracted cDNA library enriched between oviparous and ovoviviparous *Artemia* ovisacs. Among them, a shell gland-specifically expressed gene (*SGEG*) has been found to be involved in the cyst shell formation. Lacking SGEG protein (by RNA interference) caused the cyst shell to become translucent and the chorion layer of the shell to become less compact and pultaceous and to show a marked decrease of iron composition within the shell. The RNA interference induced defective diapause cysts with a totally compromised resistibility to UV irradiation, extremely large temperature differences, osmotic pressure, dryness, and organic solvent stresses. In contrast, the natural cyst would provide adequate protection from all such factors. *SGEG* contains a 345-bp open reading frame, and its consequentially translated peptide consists of a 33-amino acid residue putative signal peptide and an 81-amino acid residue mature peptide. The results of Northern blotting and *in situ* hybridization indicate that the gene is specifically expressed in the cells of shell glands during the period of diapause cyst formation of oviparous *Artemia*. This investigation adds strong insight into the mechanism of cyst shell formation of *Artemia* and may be applicable to other areas of research in extremophile biology.**

Salt lakes on plateaus, are widely known as "seas of death," because they represent one of the most hostile environments on the earth in terms of extreme salinity, high pH, anoxia, large temperature differences, and intermittent dry conditions. Hardly any animal can survive such extremes. However, one notable exception lies in the shape of a small crustacean, *Artemia.*

Artemia, also called the brine shrimp, is an ancient species that first appeared ~400 million years ago (1). To cope with harsh and complex habitats such as salt lakes, *Artemia* are able, when the circumstances become adverse, to release their offspring into a dormant, encysted state, rather than simply releasing swimming nauplius, to ensure survival. Such adverse conditions include environments where the *Artemia* may experience high salinity, low oxygen levels, short days, or conditions of extreme temperature variation (2, 3). These dormant cysts will keep diapause until the state is terminated by activation (triggered by factors such as desiccation, dehydration, cold or chemical treatment), at which point they resume development when appropriate and stable environmental conditions have arisen (4–7).

The diapause cysts, with their greatly reduced metabolic activity, contain embryos existing as late gastrulae and are composed of ~4000 cells that are arrested at the G_2/M phase with a complete turning off of RNA and protein synthesis (8, 9). Previous studies indicate that the resistance and resumption ability of *Artemia* cysts have several causes. In addition to the arrested cell cycle, it has been noted that large amounts of two molecular chaperone proteins, namely p26 and artemin, are synthesized (10–12), and a high concentration of trehalose is also accumulated (13–15). Moreover, a complicated enzyme system is also involved in the diapause and resumption mechanism, including AMP-activated protein kinase (16) and p90 ribosomal S6 kinase regulatory pathway (17–19).

In addition to falling into diapause, *Artemia* themselves secrete a rigid noncellular shell to cope with the extreme environmental stresses before they release the diapause cysts. The complex noncellular cyst shell consists of two main regions; the outer region, secreted by the shell gland, is of hypochlorite-soluble chorion, whereas the hypochlorite-resistant inner region is formed by blastoderm cells and comprises the embryonic cuticle (5, 20, 21). The shell glands, which are composed of clusters of secretory cells, are situated at the ovisac and open into the uterus. There are many dark brown secretory granules, which probably contain chorion material and pigments such as hematin formed in the cells of the shell glands at the point where the oocytes emerge in the ovaries during the reproductive period. These are secreted out at the second day after the oocytes enter the uterus. Therefore the shell glands vary from

* This work was supported by National Natural Sciences Foundation of China Grants 40730212 and 40876069 and 863 Program of China Grant 2007AA09Z426.

[S] The on-line version of this article (available at http://www.jbc.org) contains supplemental Figs. S1 and S2.

[1] To whom correspondence should be addressed: Institute of Cell Biology and Genetics, College of Life Sciences, Zhejiang University, Zijingang Campus, Hangzhou, Zhejiang 310058, China. Tel.: 86-571-88273176; Fax: 86-571-88273176; E-mail: w_jyang@cls.zju.edu.cn.

dark brown to white, even to colorless, as reproductive cycles differ (22, 23).

Microphotographs shot by Sugumar and Munuswamy (24) reveal that both the chorion and the embryonic cuticle have an exquisite structure (21). Chorion consists of two distinct layers. First, a compact outer covering is over the cyst with many radially aligned aeropyles penetrating through. This is known as the cortical layer. Second, in a cavernous region below the cortical layer is the alveolar layer, which may act as a float for the newly laid cysts. A thin supra cortical layer, probably consisting of cuticulin, covers the outer surface of the cortical layer. The embryonic cuticle, which is impermeable to nonvolatile solutes, is otherwise composed of a broad multilamellar region as a fibrous layer sandwiched between the outer and inner cuticular membranes and constructed as a tripartite structure. This forms an area of relative independence from the external environment and serves to maintain the homeostasis of inorganic ions (2). The molecular formulation of the cyst shell is complex, and details remain unclear, although it is known that the cyst shell does contain chitin, lipoprotein, hematin, and some metal elements (25–27).

Besides preventing mechanical damage (28), the cyst shell also plays an important role in protecting the embryo within from other lethal environmental stresses. Previous experimental data have confirmed the protective capabilities of the cyst shell. Tanguay *et al.* (29) indicated that the hatching rate of intact cysts is significantly higher than the decapsulated ones after ultraviolet irradiation treatment. Hematin, the hemopigment of the cyst shell, is also demonstrated to have a light-screening function (27). Clegg (30) indicated that the cyst shell plays a critical role in desiccation tolerance, because the rate of dehydration of decapsulated cysts is much higher than intact ones in the dehydration study, and rapid water loss significantly reduces the hatching level of dehydrated cysts. Liu *et al.* (31) also found that intact cysts have better thermotolerance than decapsulated ones in both dry and water heating studies.

In our experiments, through the *in vivo* gene knockdown by RNA interference, a shell gland-specifically expressed gene (*SGEG*) has been found to be involved in the cyst shell formation. The formed cyst shell has been demonstrated to play an important role in resistance to UV irradiation, large temperature differences, osmotic pressure, dryness, and organic solution stresses.

EXPERIMENTAL PROCEDURES

Culture of Artemia parthenogenetica and Tissue Sample Collection—The oviparous *Artemia* were reared in 8% (w/v) artificial seawater (Blue Starfish, China) under light and dark cycles of 4 h (12:00–16:00) and 20 h, respectively. Otherwise the ovoviviparous *Artemia* were reared in 3% (w/v) artificial seawater under light and dark cycles of 16 h (7:00–23:00) and 8 h, respectively. The water temperature was kept at 28 °C. *Chlorella* powder was supplemented as brine shrimp food (Fuqing King Dnarmsa Spirulina Co. Ltd., Fuqing, China).

A sufficient amount of both oviparous and ovoviviparous *Artemia*, at the stage where oocytes are stored in lateral pouches (the stage usually only lasting less than 6 h), were collected and temporarily cultured. Both types were used for isolating ovisacs each day throughout the reproductive cycle (for 5 days). The collected ovisacs were marked as either oviparous or ovoviviparous samples, and the day of collection was noted (from day 1 to day 5).

The *Artemia* used for isolating ovisacs were placed in an ice bath for 1–2 min until they were lightly anesthetized. Then the ovisac was dissected, snap-frozen in liquid nitrogen, and stored at −80 °C until RNA preparation.

Total RNA Extraction, cDNA Synthesis, and Suppression Subtractive Hybridization—The total RNAs of both oviparous and ovoviviparous ovisacs were extracted individually by TRIzol reagent (Invitrogen). One microgram of each total RNA was used to synthesize the first strand cDNA by PowerScript™ reverse transcriptase (Takara Bio Company, Otsu, Japan) at 42 °C for 90 min, and two adaptors were added to both endings by 3′ SMART CDS Primer II A and SMART II A Oligonucleotide (Super SMART™ PCR cDNA synthesis kit; Takara Bio Company, Japan). The first strand cDNAs, purified by NucleoSpin® columns, were amplified using 5′ PCR Primer II A for optimized cycles, and the double-stranded cDNAs were finally purified by NucleoSpin® columns once again.

For SSH,[2] the double-stranded cDNAs of oviparous ovisac samples from day 1 to day 5 were mixed in equal parts as a tester, whereas the double-stranded cDNAs of ovoviviparous ovisac samples from day 1 to day 5 were mixed in equal parts as a driver. The subtractive library was then generated using the Clontech PCR-Select cDNA subtraction kit (Takara Bio Company), according to established protocols. After two cycles of hybridization and two cycles of PCR amplification, a total of 84 individual recombinant clones in pUCm-T vector (Bio Basic Inc., Markham, Canada) were picked and used as templates for PCR amplification using vector primers M13F and M13R. Each PCR product (1 μl) was spotted onto a nylon membrane (Hybond-N; Amersham Biosciences), hybridized with the probes of tester and driver cDNA in order, and detected by the DIG chemiluminescent detection system (DIG High Prime DNA labeling and detection starter kit II; Roche Applied Science).

RACE and Sequence Analysis—All of the clones that exhibited distinct expression differences according to the result of SSH were sequenced (Sangon, Shanghai, China). One full-length cDNA of them (*SGEG*) was achieved by 3′- and 5′-RACE methods.

The gene-specific primers CRaceF for 3′-RACE and CRaceR for 5′-RACE (Table 1) were designed based on the nucleotide sequences of *SGEG*, and the cDNAs for RACE were synthesized from the total RNA of oviparous ovisacs. All of the processes of 3′- and 5′-RACE were following the manufacturer's protocol of FirstChoice™ RLM-RACE kit (Ambion, Austin, TX). The sequenced cDNA was analyzed by using Lasergene software (DNAStar Inc.), and the deduced amino acid sequence of the peptide was predicted by the PredictProtein and Scratch Protein Predictor website. Otherwise the Blast (blastx and blastn)

[2] The abbreviations used are: SSH, suppression subtractive hybridization; DIG, digoxingenin; RACE, rapid amplification of cDNA ends; ds, double-stranded; RNAi, RNA interference; SEM, scanning electron microscope; FE-SEM/EDS, field emission SEM/energy dispersive system.

TABLE 1

Nucleotide sequences and positions of primers used in polymerase chain reactions

F and R indicate the forward and reverse directions, respectively. The underlined regions represent the adscititious recognition sequences of restriction endonucleases.

Primer	Length	Position	Direction	Sequence (5′ → 3′)
	bp			
CRaceF	20	273–292	F	TTTGACGGACACCAACTTAG
CRaceR	20	121–140	R	TTCTTTGGCAGCTTCCTCTG
CExpF	30	37–57	F	CGCGGATCCATGGGGGTAAAGGAAGTTTTG
CRiR	31	410–432	R	GCTCTAGACTAAATTTGCATCTGTTTAATCC
CExpR	30	400–420	R	CCGCTCGAGCTGTTTAATCCAGTAAGCAAC
GFPF	30	122–144	F	GGAATTCAACTTACCCTTAATTTTATTTGC
GFPR	28	461–480	R	GCTCTAGAGCCATTCTTTGGTTTGTCTC
CQF	20	121–140	F	CAGAGGAAGCTGCCAAAGAA
CQR	20	273–292	R	CTAAGTTGGTGTCCGTCAAA
TubF	20	532–551	F	TCTACTGCCGTTGTTGAGCC
TubR	20	694–713	R	ATGGAGGAAACGATTTGACC

program was performed using the NCBI website. The nucleotide sequence of *SGEG* was submitted to GenBank™ under the accession number EU683079.

RNA Interference—A pair of primers (CExpF and CRiR in Table 1) were designed for the preparation of *SGEG* dsRNA. A 361-bp cDNA fragment was subcloned into the plasmid pET-T7 (17) at XbaI and EcoRI sites (the EcoRI site exists in the *SGEG* sequence, positions 72–77). For negative control, a 359-bp *GFP* cDNA fragment was amplified using the primers GFPF and GFPR (Table 1) and subcloned into the pET-T7 vector at the same restriction sites. The recombinant plasmids were transformed into *Escherichia coli* HT115, and the dsRNAs were produced and purified as described by Yodmuang *et al.* (32).

Based upon the basic and quantitative controls (supplemental Fig. S1), 300 ng of *SGEG* dsRNA was injected into the reproductive segments of *Artemia* at the instar XII stage (before ovarian development). An UltraMicroPump II equipped with the Micro4™ microsyringe pump controller was used for the microinjection. Both RNAi and control *Artemia* were cultured in 8% artificial seawater under the condition of light/dark cycles of 4/20 h. The RNAi-induced and control cysts were observed by light microscopes and collected for the following experiments.

Real Time PCR—Total RNAs were extracted from ovisacs (lateral pouches filled with oocytes) of RNAi-induced *Artemia* and controls. After reverse transcription, all real time PCRs were performed on the Bio-Rad MiniOpticon™ real time PCR System using the SYBR® Premix Ex Taq™ (Takara Bio Inc.) and 200 nM *SGEG*-specific primers (CQF/CQR and TubF/TubR in Table 1). Relative transcript levels are presented as fold change calculated using the comparative C_T method as described by Livak and Schmittgen (33, 34) with α-tubulin cDNA as the internal reference. All of the data are given as the means ± S.E. of independent experiments from six separate RNA pools. All statistical analyses were performed using the one-way analysis of variance, and the difference was considered significant for $p < 0.01$.

Transmission Electron Microscope (TEM), Scanning Electron Microscope (SEM), and Field Emission SEM/Energy Dispersive System (FE-SEM/EDS) Analysis—A transmission electron microscopic study was carried out to search for differences between the shells of RNAi-induced and those of control cysts, following the method described by Hofmann *et al.* (35). Both cysts were nicked and fixed in 2.5% glutaraldehyde prepared in 3% NaCl for 12 h. Then they were washed and postfixed in 1% osmium tetroxide in 3% NaCl solution, dehydrated in graded acetone series, and embedded in spurr resin. Sections of ~70 nm were cut with microtome (UC6; Leica), stained with 2% uranyl acetate and Reynold's solution (0.2% sodium citrate and 0.2% lead nitrate), then viewed in a transmission electron microscope (JEM-1230; JEOL), and photographed at a voltage of 70 kV.

For SEM and FE-SEM/EDA analysis, the RNAi-induced and control cysts were individually fixed by 2.5% glutaraldehyde for 2 h. Then these cysts were washed and dehydrated in graded acetone series and critical point dried with CO_2 using a critical point dryer (Hitachi HCP-2). These were used for FE-SEM/EDS (Sirion SEM System, FEI Co., Hillsboro, OR) analysis directly or sputter-coated with gold (Hitachi E-1010) for scanning electron microscopy (Hitachi S-3000N).

SDS-PAGE and Western Blotting—Equal numbers of the RNAi induced and control cysts were homogenized in 8 M urea individually and boiled for 10 min. After centrifugation to remove insoluble shell fragments, the supernatants were quantified using the Bradford method (36). Twenty micrograms of protein of each sample were electrophoresed on 15% polyacrylamide gels and detected by Coomassie Brilliant Blue.

The open reading frame of *SGEG* cDNA was amplified using the primers CExpF and CExpR (Table 1) and cloned into the pET-32 vector with an N-terminal His_6 tag. Recombinant SGEG protein was expressed in *E. coli* BL21 (DE3) and purified by nickel-nitrilotriacetic acid-agarose (Qiagen), and the anti-SGEG antibody was raised in rabbit (HuaAn Biotechnology Co. LTD.). Fifty micrograms of protein of each sample were separated on 12.5% SDS-PAGE gels and transferred to polyvinylidene difluoride membranes (Millipore) for Western blotting analysis. The membranes were incubated with anti-SGEG antibody and anti-α-tubulin antibody (Beyotime, Shanghai, China) overnight at 4 °C and detected using the BM Chemiluminescence Western blotting kit (Roche Applied Science).

Tests of Resistance of Environmental Stresses for RNAi-induced Cysts—A sufficient number of RNAi-induced and control cysts were collected for the anti-environmental stress test, which included dryness, UV irradiation, high temperature, freezing, extreme osmotic pressure, and organic solvent tests. Triplicate experiments were performed for each of these physiological stresses.

For the test of dryness, both the RNAi-induced and control cysts were air dried and kept at room temperature with continual observation. For the UV irradiation test, both the RNAi-induced and control cysts were exposed to ultraviolet light (~310 nm) for 3.6 J/cm^2. For the high temperature and freezing stress test, the RNAi-induced and control cysts were incubated in the water bath at 50 °C for 5 min or frozen at −30 °C for 3 days. For the test of coping with extreme osmotic pressure, the RNAi-induced and control cysts were soaked in 6 M NaCl for 450 min or in deionized water for 3 days.

After the above tests, all RNAi-induced cysts were incubated in 3% artificial sea water with continual illumination at 25 °C for

hatching. The hatching rates were then investigated for a period of 72 h. In contrast all the control cysts were activated before hatching by soaking in saturated brine for 24 h and freezing in −20 °C for 3 months. In addition, for the test of resistance to organic solvent, both the RNAi-induced and activated control cysts were incubated in 3% artificial sea water with 0.5 M methanol for investigating hatching rates.

Northern Blotting Analysis—A DIG-labeled cDNA fragment (384 bp) was amplified using the primers CExpF and CExpR (Table 1) and used as a probe for the Northern blotting analyses. The total RNA of both oviparous and ovoviviparous *Artemia*, the total RNA of both thoracic segments and ovisacs of oviparous *Artemia*, and the total RNA of oviparous ovisacs from days 1–5 were extracted. All of the samples (15 μg corresponding to each tissue) were separated by agarose gel electrophoresis, then transferred to a nylon membrane (Hybond-N; Amersham Biosciences) for overnight hybridization at 45 °C, washed twice at 55 °C, and finally detected by the DIG chemiluminescent detection system (Roche Applied Science).

In Situ Hybridization—The DIG-labeled sense and antisense RNA probes, corresponding to nucleotides 80–432 of SGEG cDNA, were amplified (primed by CExpF and CExpR; Table 1) and cloned into plasmid vector pSPT18 at EcoRI and XbaI sites (the EcoRI site exists in the *SGEG* sequence). They were then transcribed *in vitro* from the EcoRI- and XbaI-linearized templates, respectively (according to the manufacturer's instruction of DIG RNA Labeling kit SP6/T7; Roche Applied Science).

For tissue slice preparation, *Artemia* were anesthetized as mentioned previously, snap-frozen in liquid nitrogen, and embedded in Tissue-Tek™ (Sakura Finetechnical Co. Ltd). Then 10-μm-thick frozen sections were prepared by frozen ultramicrotome.

Dry sections were fixed with paraformaldehyde, digested with proteinase K and hybridized at 42 °C overnight. Then these slices were washed at 52 °C and blocked by blocking solution (Roche Applied Science). They were then treated with anti-DIG-AP conjugate (Roche Applied Science; 1:500) and visualized with the colorimetric substrates nitroblue tetrazolium/5-bromo-4-chloro-3-indolylphosphate (Promega) according to the manufacturer's instructions. Finally, the photographs were taken on an inverted microscope (ECLIPSE TE2000-S; Nikon).

RESULTS

Gene Screening and Identification of SGEG—A SSH library was constructed, and the double-stranded cDNA from oviparous and ovoviviparous ovisacs of *Artemia* were used as tester and driver, respectively. Eighty-four clones were obtained from the SSH library enriched for the oviparous-specific transcripts. Twenty-two clones exhibiting distinct expression differences were selected for sequencing and obtaining of the complete cDNA sequence by RACE. A differentially expressed gene, which contained a 450-bp complete cDNA sequence, was the focus, and this was named the shell gland-specifically expressed gene (*SGEG*). The conceptually translated peptide from the gene consists of a 33-amino acid putative signal peptides and an 81-amino acid putative residue mature peptides (supplemental Fig. S2). It was considered to be a novel gene, having no apparent identity with other known genes or proteins when alignments were compared with sequences in the DDBJ/EMBL/GenBank™ data base.

In Vivo Knockdown of SGEG by RNAi in Artemia—RNA interference was performed by dsRNA microinjection into the Artemia at instar XII stage, and the *SGEG* transcript level was reduced to less than 20% (Fig. 1*A*).

Although both the RNAi and control *Artemia* showed no significant abnormal phenotypes, the cysts, which were oviposited by RNAi-treated *Artemia*, stuck on bottom of the culture tank having a characteristically soft cyst shell in direct contrast to control cysts, which could be observed sinking, floating, and suspended in the same tank. For the RNAi-induced cysts, more than 20% were found to be able to develop into swimming nauplii by 72 h without any activation necessary. The control cysts remained unable to be hatched out directly without a procedure of diapause termination even in the presence of appropriate hatching conditions.

The observations using the inverted microscope revealed that the shells of RNAi-induced cysts were transparent, whereas the control cysts remained opaque. Thus the embryo and blastopore inside could be observed clearly for the RNAi-induced cysts (Fig. 1*B*, *panels a* and *a′*). Moreover, in contrast to the control cyst shell, the RNAi-induced cyst shell had changed to light yellow when observed by anatomical microscopes (Fig. 1*B*, *panels b* and *b′*).

Furthermore, the cortical layer and alveolar layer (chorion layer) of the RNAi-induced cyst shell was contorted and obviously lighter (more electron-transparent) than that of control cysts as shown in the transmission electron micrographs (Fig. 1*C*, *panels a* and *a′*). In addition, in the RNAi-induced cysts, the thin supra cortical layer had disappeared, the aeropyles in the cortical layer were blurry and syncretized, and the cortical layer of RNAi-induced cyst shell was less than half the thickness of the control cortical layer (Fig. 1*C*, *panels b* and *b′*).

The scanning electron micrographs revealed that the shell surface of cysts reproduced by RNAi-treated *Artemia* was lamellar and rough (Fig. 1*D*, *panel a*), instead of the compact and smooth shell of the control cyst (normal cortical layer; Fig. 1*D*, *panel a′*). However, the inner alveolar layer of the RNAi-induced cyst showed no difference, in contrast with the control cyst (Fig. 1*D*, *panels b* and *b′*).

The results of FE-SEM/EDS showed the main metal elemental contents difference between RNAi-induced and control cysts. This indicated that the iron content of RNAi-induced cysts was sharply decreased in comparison with control cysts; however, the kalium content was higher (Fig. 2).

Otherwise, the SDS-PAGE gel showed that several specific proteins of RNAi-induced cysts were down-regulated (≥66, 27, 25, 17, and 10 kDa), whereas several proteins were up-regulated (49, 47, and 19 kDa) (Fig. 3*A*). The results of Western blotting showed that the SGEG protein was significantly decreased in the RNAi-induced cysts relative to control cysts and present in the diapause cysts (Fig. 3*B*). The molecular mass of the detected protein is ~14 kDa, similar to the predicted molecular mass of SGEG protein.

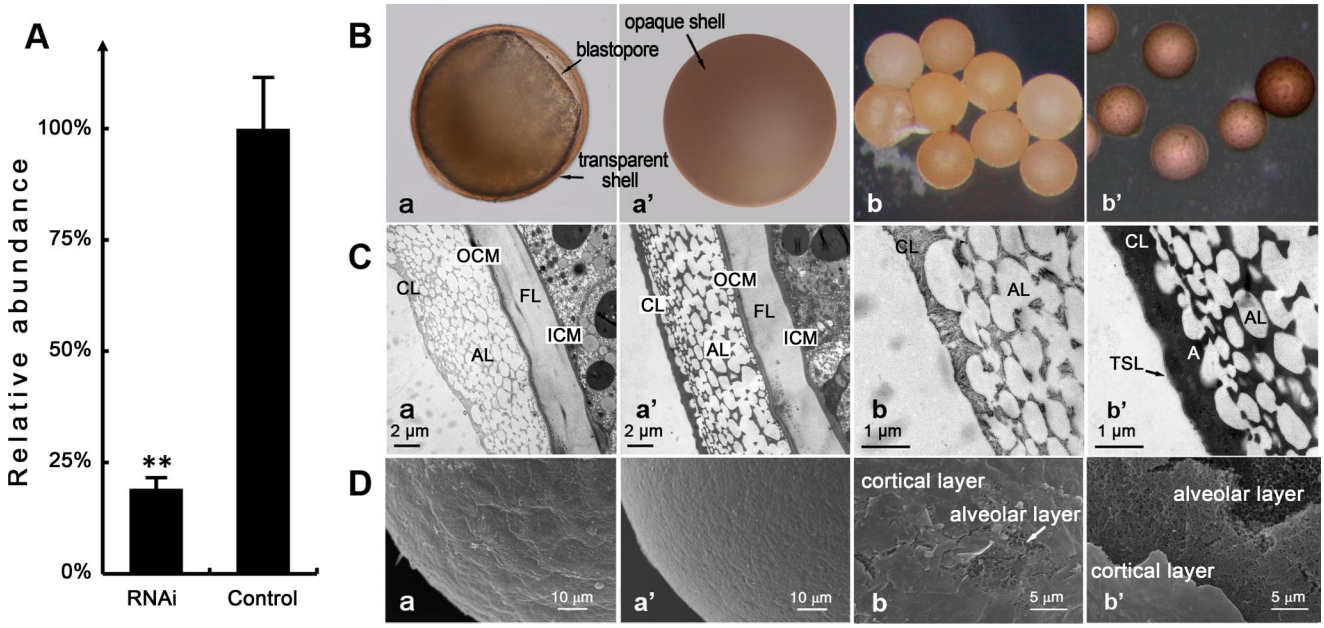

FIGURE 1. **Differences between *SGEG* RNAi-induced cysts and control cysts.** *A*, detection of relative *SGEG* transcript level in test and control groups was by real time PCR. Each *Artemia* was microinjected with 300 ng of *SGEG* dsRNA (tests) or *GFP* dsRNA (controls). The content of *SGEG* cDNA in the control sample (total RNA of the ovisacs) was defined as 100%. All of the data are given as the means ± S.E. The *asterisks* indicate a highly significant difference ($p < 0.01$) between the test and the control group as analyzed by one-way analysis of variance. *B*, light micrographs. *Panel a*, *SGEG* RNAi-induced cyst (by inverted microscope, ×400); *panel a'*, control cyst (by inverted microscope, ×400); *panel b*, *SGEG* RNAi-induced cyst (by anatomical microscope, ×80); *panel b'*, control cyst (by anatomical microscope, ×80). *C*, transmission electron micrographs. *Panel a*, the cyst shell of RNAi-induced cyst, ×8000; *panel a'*, cyst shell of control cyst, ×8000; *panel b*, cortical and alveolar layer of RNAi-induced cyst, ×30000; *panel b'*, cortical and alveolar layer of control cyst, ×30000. *CL*, cortical layer; *AL*, alveolar layer; *OCM*, outer cuticular membrane; *FL*, fibrous layer; *ICM*, inner cuticular membrane; *TSL*, thin supra cortical layer; *A*, aeropyle. *D*, scanning electron micrographs. *Panel a*, cortical layer of RNAi-induced cyst, ×1000; *panel a'*, cortical layer of control cyst, ×1000; *panel b*, alveolar layer of RNAi-induced cyst, ×3000; *panel b'*, alveolar layer of control cyst, ×3000.

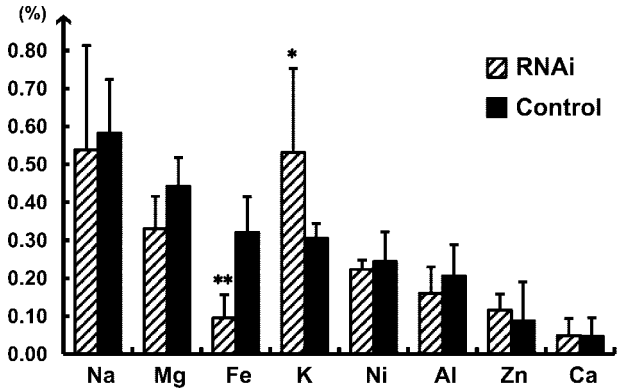

FIGURE 2. **The metallic elemental compositions of cyst shells of two groups of cysts.** The RNAi group is indicated by *hatched bars*, and the control group is indicated by *solid bars*. The results are expressed as the means ± S.E. of independent measured values from different cysts ($n = 6$). The *asterisks* indicate significant differences. *, means $p < 0.05$; **, means $p < 0.01$.

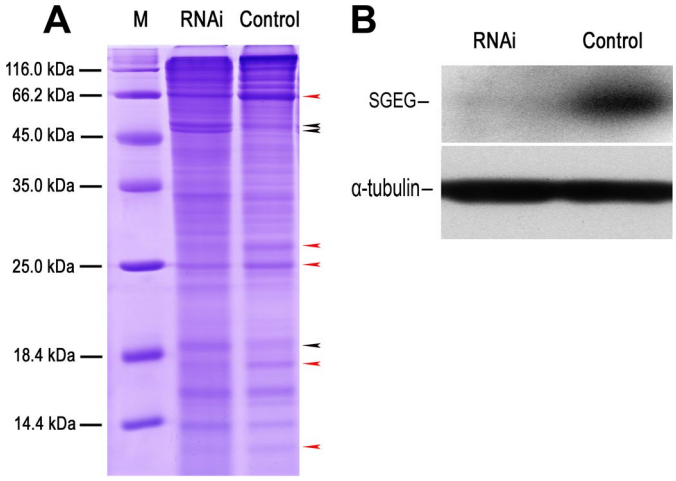

FIGURE 3. **SDS-PAGE and Western blotting of RNAi-induced and control cysts.** *A*, SDS-PAGE gel stained by Coomassie Brilliant Blue. Each lane contains 20 μg of total protein. The *red arrows* indicate the down-regulated proteins in RNAi sample, and the *black arrows* indicate the up-regulated proteins. The molecular mass marks are indicated on the *left side*. *B*, Western blotting with antibody against SGEG protein. α-Tubulin is used for loading control. Each lane contains 50 μg of total protein.

Resistance Tests of RNAi-induced Cysts toward Environmental Stresses—As mentioned in the Introduction, the natural cyst shell of *Artemia* provides strong resistance toward major environmental stress, including dryness, osmotic pressure, temperature change, UV exposure, organic solvent exposure, and others. However, in our experiments, in each case such resistance ability of RNAi-induced cysts was found to be highly compromised.

Fig. 4*A* exhibited the appearance of RNAi-induced cysts during the gradual change caused by air drying at room temperature. The RNAi-induced cysts started shrinking after 1 h and were completely atrophic 4.5 h later. The same phenomenon could be observed in the hyperosmotic pressure test, showing that the embryos shrank drastically after 1 h in 6 M NaCl solution and the majority of cellular water was lost by 7.5 h. However, the control cysts kept their round shape all along (Fig. 4*B*). Likewise, we found that the RNAi-induced cysts were unable to survive in the hypoosmotic pressure environment. Most of the RNAi-induced cysts burst when incubated in fresh water for 3 days, and the embryos inside leaked out, whereas the normal

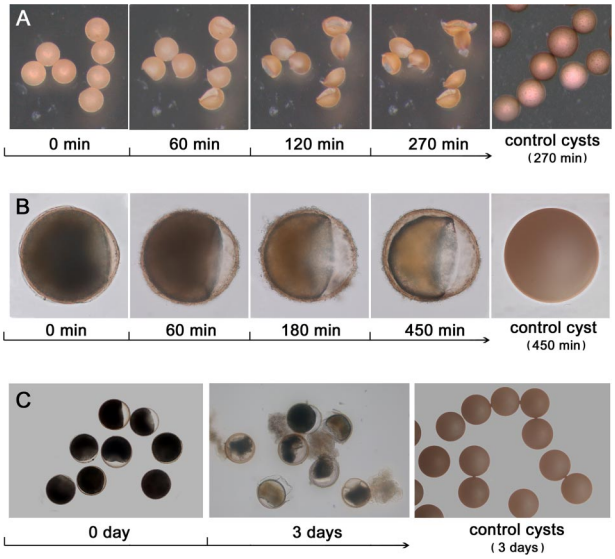

FIGURE 4. **Resistance tests of the RNAi-induced cysts toward various environmental stresses.** *A*, photomicrographs of RNAi-induced and control cysts in air drying test from 0 to 270 min (by anatomical microscope, ×80). *B*, photomicrographs (by inverted microscope, ×400) of RNAi-induced and control cysts having been soaked in 6 M NaCl solution from 0 to 450 min. *C*, photomicrographs (by inverted microscope, ×100) of RNAi-induced and control cysts that were soaked in deionized water for 3 days.

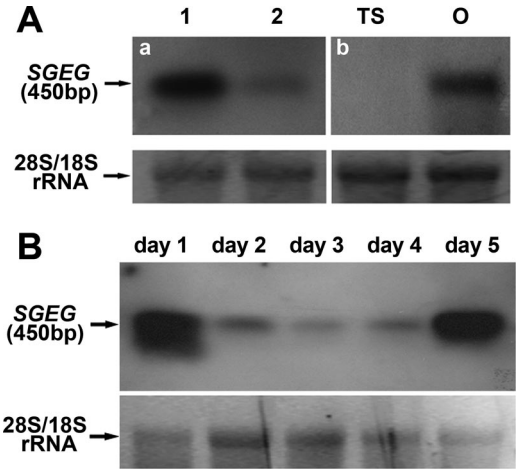

FIGURE 5. **Northern blot analysis of the characters of *SGEG* expressed.** *A*, Northern blot analysis of the location of *SGEG* expressed. This shows that *SGEG* is specially expressed in the ovisacs of oviparous *Artemia*. *Panel a*, The total RNA samples of oviparous *Artemia* (*line 1*) and ovoviviparous *Artemia* (*line 2*) are loaded. *Panel b*, the total RNA samples of thoracic segments (*TS*) and ovisacs (*O*) of oviparous *Artemia* are loaded. *B*, Northern blot analysis of expression of *SGEG* throughout an oviparous developmental cycle (ovisac samples day 1 to day 5). It shows that abundant accumulations of the mRNA were observed only in samples from day 1 and day 5. The ethidium bromide-stained 28 S/18 S rRNA bands were used as a control for loading variation. A 384-bp *SGEG* sequence was amplified and DIG-labeled as probe.

control cysts remained completely uninjured (Fig. 4*C*). In addition, the hatching rate of RNAi-induced cysts was higher than 20%, but the cysts, which suffered stresses of UV irradiation (3.6 J/cm^2 ~310 nm), high temperature (water bath at 50 °C for 5 min), and organic solvent (hatching in 0.5 M methanol), were unable to hatch. Also, the hatching rate of frozen RNAi-induced cysts (−30 °C for 3 days) declined to 6%, where, in contrast, the control cysts maintained a normal hatching rate (~75%) after such environmental stresses.

Expression Characterization and Localization of SGEG—The result of Northern blotting analysis demonstrated that the *SGEG* mRNA only significantly accumulated in oviparous *Artemia* (Fig. 5*A*, *panel a*), or, more specifically, only in the oviparous ovisac (Fig. 5*A*, *panel b*). In contrast the signal detected in ovoviviparous *Artemia* was very weak. Furthermore, the expression period of *SGEG* was examined throughout a oviparous developmental cycle (from ovulation to oviposition, 5 days), and the results indicated that the mRNA of *SGEG* is only abundantly accumulated during the first day when oocytes are temporarily stored in lateral pouches (*day 1* in Fig. 5*B*; see also details in the section regarding sample collection) and the day before diapause cysts are released (*day 5* in Fig. 5*B*; meanwhile the oocytes are mature in ovaries, and the next reproductive cycle has started).

The result of *in situ* hybridization indicated the cellular location of *SGEG* mRNA in the ovisacs of oviparous *Artemia*. As shown in Fig. 6, clear signals from *SGEG* mRNA were observed only in the secreting cells of the shell glands (Fig. 6*A*). The signal was absent when hybridization was done with a sense control probe (Fig. 6*B*).

DISCUSSION

The cyst shell of *Artemia* is an exquisite multi-layered construction that gives the diapause embryo its strong resistance to severe environmental stress. However, what the cyst shell is synthesized from and how it is formed have remained largely unknown. In this research, a novel gene (*SGEG*), involved in the formation of the cyst shell was screened from the subtractive library of ovisacs of oviparous and ovoviviparous *Artemia*, and its expression characteristics and function were confirmed.

Prediction of the Structure of SGEG Protein—Although the SGEG protein has no apparent identity with other known proteins, its secondary and tertiary structures were predicted. Residues 1–33 are predicted as a signal peptide. The putative mature protein contains two putative α-helix regions (comprising residues 36–41 and 45–54) and four putative β-sheet regions (comprising residues 69–73, 76–79, 89–93, and 99–102). Also, three putative casein kinase II phosphorylation sites (residue positions Thr^{60}, Thr^{83}, and Ser^{94}) and a putative *N*-glycosylation site (residue position Asn^{87}) were found in the mature protein. However, the tertiary structure of the SGEG protein could not be predicted exactly, because there is no known similar structural sequence negating the ability to build a model for prediction. Only the SCRATCH protein predictor website provided a possible tertiary structure of the SGEG protein based on energy function. Further analysis is scheduled in our ongoing research.

The Structure and Formulation Changes of Cyst Shell Induced by RNAi—The assertion that *SGEG* is closely related to the formation of cyst shells was mainly deduced from the result of RNA interference, in that both the structure and formulation of the cyst shell was changed dramatically after the silencing of *SGEG* mRNA. On the observations with light microscopes, SEM, and transmission electron microscopic, the RNAi-induced cyst shell becomes transparent, incompact, and pultaceous. We therefore presume that some substances within the normal chorion layer are lacking.

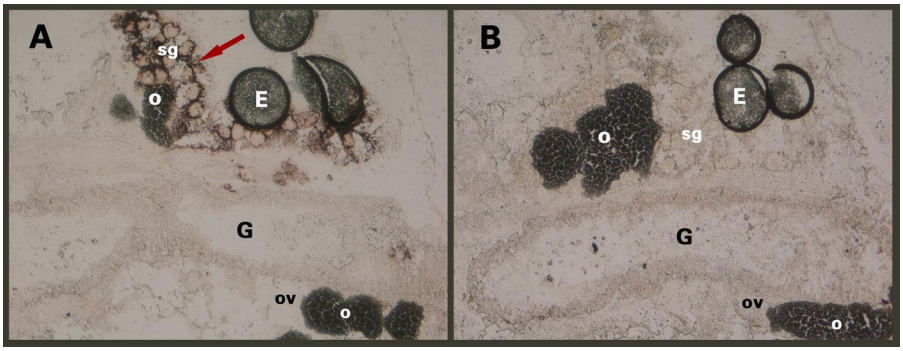

FIGURE 6. **Localization of mRNA in ovisac of oviparous *Artemia*.** The 361-bp DIG-labeled sense and antisense RNA probes were used for *in situ* hybridization. The distribution of the purple signals at cells of shell glands are indicated by *red arrow* (*A*). No hybridization signal was observed with sense cRNA probe (*B*). *G*, gut; *E*, embryo; *ov*, ovary; *sg*, shell gland; *o*, oocyte (cross-section, ×100).

In addition to such changes of appearance, the results of FE-SEM/SED and SDS-PAGE also show that the formulations of the cyst shell are obviously changed after RNA interference. Van der Linden *et al.* (27) suggested that a light-screening iron-binding hemopigment, hematin, is located in the cyst shell. By coincidence, the RNAi-induced shell not only became transparent, but the result of FE-SEM/EDS also indicated that the iron content had also sharply decreased (Fig. 2). It is possible this implies that the ultrahigh transmittance of the cyst shell is caused by the loss of hematin.

However, we noticed an interesting phenomenon in that there were still many dark brown secretory granules existing in the shell glands cells when the oocytes emerged. Considering Dutrieu (23), who mentioned that hematin was excreted via shell glands, we presume that all or some of the shell materials are still synthesized in shell glands, but cannot accumulate in the cyst shell when *SGEG* has been silenced.

Physiological Changes of the RNAi-induced Cysts—Along with changes of structure and formulation of the cyst shell, the physiology of diapause cysts also changed after RNA silencing. The natural cyst is known to be unable to hatch out immediately after oviposition, being kept at the state of diapause until accepting the signals of diapause termination. These signals include freezing, dehydration, darkness, and elevated CO_2. The diapause termination process also is called "activation" (4, 5). The adiabatic, impermeable, and opaque natural cyst shell ensures that the diapause state is only to be terminated when the signals have lasted for a long period (usually for months). This is a protective mechanism of *Artemia* to evade the adversities, such as the dry season or winter. However, we found that more than 20% of the RNAi-induced cysts would hatch into normal larvae under appropriate conditions in absence of activation. We presume that the abnormal hatching rate of RNAi-induced cysts probably relates to the incompact cyst shell. Because the permeable and transparent shell allows the embryos inside easier access to the light, oxygen, and water that are necessary for development, the RNAi-induced embryos can develop into a later stage without diapause, or the state of diapause can be terminated after a very short time.

More interestingly, the result of hatching rate experiments showed that the RNAi-induced cysts were sensitive to environmental stresses, such as dryness, high temperature, freezing, osmotic pressure, UV irradiation, and the presence of organic solvents. This implies that the SGEG protein is related to the resistance toward such environmental stresses upon the cyst shell. When *SGEG* was silenced by RNAi, the exquisite protective mechanism of the chorion layer was compromised. In detail, first, the water and organic solvent was able to freely penetrate the RNAi-affected cyst shell. In addition to the rarefaction, the change of permeability may result from the abnormal aeropyles in the cortical layer of the affected cyst shell (Fig. 1*C*, *panels b* and *b′*). Thus when the RNAi-induced cysts were dried in air and soaked in 6 M NaCl solution or 0.5 M methanol, the embryos inside would die because of rapid water loss, an imbalance of osmotic pressure, or the cytotoxicity of organic solvents. Moreover, the result may have been that the pores of the alveolar layer were filled with brine from the external environment as would be the case for the permeable cortical layer. This would likewise result in the easy transmission of external heat conducted to the embryo, resulting in death in the high temperature test. Second, the physical protection role of the cyst shell was compromised. The RNAi-induced cysts readily shrank or burst when air dried or soaked in fresh water, indicating the further deficiency of the cyst shell (Fig. 4). Likewise, the role of light-screening of the cyst shell was totally lost because of the scarcity of pigmentation, thus the abnormal cyst shell also failed to protect the embryo from UV irradiation. Also, the RNAi-induced cysts seemed to lack the most important molecular chaperones (artemin and p26), two proteins that play critical roles in cyst resistance by the results of SDS-PAGE analysis (12, 37). Such a deficiency may lead to the inability of the cysts to cope with environmental stress, especially in the areas of heat and dehydration.

Several specific proteins likewise showed a difference between RNAi-induced and control cysts in the results of SDS-PAGE (Fig. 3). The down-regulated protein in RNAi sample at 66 kDa was confirmed to be the *Artemia* yolk protein (we have determined the amino acid sequence in other research). The other down-regulated protein at 27 kDa was considered to be artemin, and the protein at 25 kDa was considered to be p26 based on molecular mass (12, 38). These two proteins are the most important molecular chaperons related to the diapause of *Artemia*. In addition, the up-regulated protein in RNAi-induced sample at 49 kDa is considered to be p49, which is a coenzyme A-transferase (39, 40) and is related to the embryonic diapause termination. All of these aspects of the regulation of protein translation imply an incomplete diapause of RNAi-induced cysts and would lead to a continuation of development a short time after oviposition.

The Expression Characteristics of SGEG—Our conclusion that *SGEG* is involved in the formation of the chorion layer of the cyst shell was also based on the special expression characteristics of *SGEG*. First, the results of Northern blotting and

in situ hybridization indicated that the gene *SGEG* is especially expressed in the cells of shell gland where the cyst shell materials are synthesized. Likewise the electron microphotographs showed that the changes caused by RNAi seem exclusively displayed and focused upon the chorion layer of the cyst shell. These observations correspond to the conclusion of Morris and Afzelius (20), who suggest that the chorion of the cyst shell is secreted by the shell gland, whereas the embryonic cuticle is formed by blastoderm cells. Second, the mRNA of *SGEG* accumulates and declines in synchrony with the synthesis of shell materials in the shell glands. That is, the mRNA of *SGEG* begins accumulation the day before ovulation, and decreases 2 days later. This is synchronous with the emergence of the brown secretory granules. Furthermore, the results of Western blotting show the SGEG protein present in the diapause cysts. Considering the dramatic change of the cyst shells, we presume that the SGEG protein may locate in the diapause cyst shell. All such evidence supports the conclusion that *SGEG* is a key gene in the formation of the diapause cyst shell.

It is known that the main aspects of the impressive resistance capacity of *Artemia* cysts are provided by their shells. Thus the chorion material of cyst shells has high potential to become an excellent biomaterial with a high number of prospective uses due specifically to such biologic characteristics. Its effective resistance toward irradiation, organic solvents, and high temperatures are of particular interest. Prospects in the fields of irradiation resistance, embryo protection, and other related areas are key areas for further study. A second potential application is that *Artemia* cysts are an important natural diet for shellfish and fish larvae, having a significant economic value in aquaculture. The cysts that are affected by gene knockdown, without a rigid shell and more readily able to hatch, may thus provide a more convenient food source than natural cysts when used as the weaning food of larvae. In conclusion, this investigation provides evidence increasing our understanding of the study of cyst shell formation of *Artemia* and may provide a new insight into other related research in extremophile biology.

Acknowledgment—We thank Chris Wood of Zhejiang University for critical reading of this manuscript.

REFERENCES

1. Dattilo, A. M., Bracchini, L., Carlini, L., Loiselle, S., and Rossi, C. (2005) *Int. J. Biometeorol.* **49,** 388–395
2. Clegg, J. S., and Trotman, C. N. A. (2002) in *Artemia: Basic and Applied Biology* (Abatzopoulos, TH. J., Beardmore, J. A., Clegg, J. S., and Sorgeloos, P., eds) pp. 129–170, Kluwer Academic Publishers, Dordrecht, The Netherlands
3. Nambu, Z., Tanaka, S., and Nambu, F. (2004) *J. Exp. Zool. Part A. Comp. Exp. Biol.* **301,** 542–546
4. Nambu, Z., Tanaka, S., Nambu, F., and Nakano, M. (2008) *J. Exp. Zool. Part A. Ecol. Genet. Physiol.* **309,** 17–24
5. Drinkwater, L. E., and Clegg, J. S. (1991) in *Artemia Biology* (Browne, R. A., Sorgeloos, P., and Trotman, C. N. A., eds) pp. 93–118, CRC Press, Boca Raton, FL
6. Lavens, P., and Sorgeloos, P. (1987) in *Artemia Research and Its Applications* (Sorgeloos, P., Bengtson, D. A., Decleir, W., and Jaspers, E., eds) pp. 27–63, Universa Press, Wetteren, Belgium
7. Versichele, D., and Sorgeloos, P. (1980) in *The Brine Shrimp Artemia, Ecology, Culturing, Use in Aquaculture* (Persoone, G., Sorgeloos, P., Roel, O., and Jaspers, E., eds) pp. 231–246, Universa Press, Wetteren, Belgium
8. Clegg, J. S. (1978) *J. Cell. Physiol.* **94,** 123–137
9. Clegg, J. S. (1997) *J. Exp. Biol.* **200,** 467–475
10. MacRae, T. H. (2003) *Semin. Cell Dev. Biol.* **14,** 251–258
11. Liang, P., Amons, R., Clegg, J. S., and MacRae, T. H. (1997) *J. Biol. Chem.* **272,** 19051–19058
12. Warner, A. H., Brunet, R. T., MacRae, T. H., and Clegg, J. S. (2004) *Arch. Biochem. Biophys.* **424,** 189–200
13. Hand, S. C., and Gnaiger, E. (1988) *Science* **239,** 1425–1427
14. Crowe, J. H., Hoekstra, F. A., and Crowe, L. M. (1992) *Annu. Rev. Physiol.* **54,** 579–599
15. Crowe, L. M., Reid, D. S., and Crowe, J. H. (1996) *Biophys. J.* **71,** 2087–2093
16. Zhu, X. J., Feng, C. Z., Dai, Z. M., Zhang, R. C., and Yang, W. J. (2007) *Stress* **10,** 53–63
17. Dai, J. Q., Zhu, X. J., Liu, F. Q., Xiang, J. H., Nagasawa, H., and Yang, W. J. (2008) *J. Biol. Chem.* **283,** 1705–1712
18. Nakanishi, Y. H., Iwasaki, T., Okigaki, T., and Kato, H. (1962) *Annot. Zool. Jap.* **35,** 223–228
19. Finamore, F. J., and Clegg, J. S. (1969) in *The Cell Cycle: Gene-Enzyme Interactions* (Padilla, G. M., Whitson, G. L., and Cameron, I. L., eds) pp. 249–278, Academic Press, New York
20. Morris, J. E., and Afzelius, B. A. (1967) *J. Ulltrastruct. Res.* **20,** 244–259
21. Clegg, J. S., Jackson, S. A., Liang, P., and MacRae, T. H. (1995) *Exp. Cell Res.* **219,** 1–7
22. Criel, G. R. J., and Macrae, T. H. (2002) in *Artemia: Basic and Applied Biology* (Abatzopoulos, TH. J., Beardmore, J. A., Clegg, J. S., and Sorgeloos, P., eds) pp. 1–38, Kluwer Academic Publishers, Dordrecht, The Netherlands
23. Dutrieu, J. (1960) *Arch. Zool. Exp. Gen.* **99,** 1–134
24. Sugumar, V., and Munuswamy, N. (2006) *Microsc. Res. Tech.* **69,** 957–963
25. Yosefali, A., Abbasali, M., and Amin, E. (1999) *Biotechnological Approach to Produce Chitin and Chitosan from the Shells of Artemia urmiana Günther, 1899 (Branchiopoda, Anostraca) Cysts from Urmia Lake, Iran*, Koninklijke Brill NV, Leiden, Holland
26. Adamkova, I. (1999) *Hatching Quality of Artemia (Artemia salina) Cysts Treated with Commercial Hypochlorite Product Savo*, Jihoceska University, Vodnany, Czech Republic
27. Van der Linden, A., Blust, R., Cuypers, K., Thoeye, C., and Bernaerts, F. (1987) in *Artemia Research and Its Applications: 2. Physiology, Biochemistry, Molecular Biology. Proceedings of the Second International Symposium on the Brine Shrimp Artemia* (Decleir, W., Moens, L., Slegers, H., Sorgeloos, P., and Jaspers, E., eds) pp. 181–188, Universa Press, Wetteren, Belgium
28. Clegg, J. S., and Conte, F. (1980) in *The Brine Shrimp Artemia* (Persoone, G. P., Sorgeloos, P., Roels, O., and Jaspers, E., eds) pp. 11–54, Universa Press, Wetteren, Belgium
29. Tanguay, J. A., Reyes, R. C., and Clegg, J. S. (2004) *J. Biosci.* **29,** 489–501
30. Clegg, J. S. (2005) *Integr. Comp. Biol.* **45,** 715–724
31. Liu, F. Q., Ji, B. C., and Xuan, C. H. (2002) *Anim. Sci. Vet. Med.* **83,** 10–11
32. Yodmuang, S., Tirasophon, W., Roshorm, Y., Chinnirunvong, W., and Panyim, S. (2006) *Biochem. Biophys. Res. Commun.* **341,** 351–356
33. Livak, K. J., and Schmittgen, T. D. (2001) *Methods* **25,** 402–408
34. Schmittgen, T. D., and Livak, K. J. (2008) *Nat. Protoc.* **3,** 1101–1108
35. Hofmann, G. E., and Hand, S. C. (1990) *J. Exp. Zool.* **253,** 287–302
36. Bradford, M. M. (1976) *Anal. Biochem.* **72,** 248–254
37. Liang, P., Amons, R., Macrae, T. H., and Clegg, J. S. (1997) *Eur. J. Biochem.* **243,** 225–232
38. Clegg, J. S., and Campagna, V. (2006) *Comp. Biochem. Phys. B. Biochem. Mol. Biol.* **145,** 119–125
39. Oulton, M. M., Amons, R., Liang, P., and MacRae, T. H. (2003) *Eur. J. Biochem.* **270,** 4962–4972
40. Zhang, J., and MacRae, T. H. (1994) *J. Biol. Chem.* **269,** 3053–3062